Fractal snapshot components in chaos induced by strong noise

Tamás Bódai,[1] György Károlyi,[2] and Tamás Tél[1]
[1]*Institute for Theoretical Physics, Eötvös University, Pázmány P. s. 1/A, Budapest, H-1117, Hungary*
[2]*Department of Structural Mechanics, Budapest University of Technology and Economics, Műegyetem rkp. 3., Budapest, H-1111, Hungary*
(Received 26 November 2010; published 1 April 2011)

In systems exhibiting transient chaos in coexistence with periodic attractors, the inclusion of weak noise might give rise to noise-induced chaotic attractors. When the noise amplitude exceeds a critical value, an extended attractor appears along the fractal unstable manifold of the underlying nonattracting chaotic set. A further increase of noise leads to a fuzzy nonfractal pattern. By means of the concept of snapshot attractors and random maps, we point out that the fuzzy pattern can be decomposed into well-defined fractal components, the snapshot attractors belonging to a given realization of the noise and generated by following an ensemble of noisy trajectories. The pattern of the snapshot attractor and its characteristic numbers, such as the finite time Lyapunov exponents and numerically evaluated fractal dimensions, change continuously in time. We find that this temporal fluctuation is a robust property of the system which hardly changes with increasing ensemble size. The validity of the Kaplan-Yorke formula is also investigated. A superposition of about 100 snapshot attractors provides a good approximant to the fuzzy noise-induced attractor at the same noise strength.

DOI: 10.1103/PhysRevE.83.046201 PACS number(s): 05.45.−a, 05.40.Ca

I. INTRODUCTION

An observed trajectory of a dynamical system is always subject to external perturbations. If the time scale of the perturbations is much shorter than that of the original signal, their effect can be modeled as noise. If a dissipative deterministic system exhibits periodic attractors and a nonattracting chaotic set, the inclusion of weak noise can give rise to an extended noisy chaotic attractor. The noise-induced chaotic attractor extends to the original attractors and the unstable manifold of the nonattracting chaotic set. A typical trajectory then visits both the original periodic attractors and the nonattracting chaotic set. This phenomenon is known as noise-induced chaos [1–3], which is fundamental in nonlinear and statistical physics and has received prolonged attention [4–7]. The field of potential applications is broad, ranging from electronic circuits [8] to epidemics [9] or population dyanmics [10].

Instead of following a long noisy trajectory, one can consider the snapshot pattern formed by many iterations of a cloud of initial conditions subject to the same sequence of random perturbations. As pointed out by Romeiras, Grebogi, and Ott [11], this pattern exhibits a clear fractal character. The idea of such snapshot attractors [11] is particularly well suited for understanding the advection of passive particles and the pattern they make in nonperiodic fluid flows [12–17]. If the flow is not exactly periodic in time, e.g., chaotic, the deviation from periodicity can be modeled as a random influence, and this perturbation flow is the same for all particles at a given instant of time. A particularly appealing example of this approach leads to a correct interpretation of the experimentally observed patterns of floaters on the surface of fluids [13]. Snapshot attractors have also been utilized to study the transition to chaos in quasiperiodically driven dynamical systems [18,19]. Recently, the effect of noise on chaotic scattering was studied also in the form of random maps [20,21]. The concept of random attractors or pullback attractors of continuous-time dynamical systems [22,23] that has appeared in recent publications on climate dynamics [24] is practically the same as that of snapshot attractors. A slight difference is that in continuous-time systems the random process is often an additive white noise. Our aim is to connect the seemingly unrelated fields of noise-induced chaos and snapshot attractors. In particular, we show that snapshot attractors can be considered as building blocks of the fuzzy noise-induced chaotic attractor for strong noise.

It is known that the details of the fractal structure of snapshot attractors vary with time, but the Kaplan-Yorke relation has been shown [11,25] to be valid in the random case under generic conditions, e.g., if none of the average Lyapunov exponents is zero [25]. Noise-induced attractors, however, exhibit strongly intermittent dynamics; it is therefore an open question how the Kaplan-Yorke value relates to the numerically accessible values of information dimension, which will be investigated here.

It is also meaningful to formulate a Kaplan-Yorke type relation involving the time-dependent finite time Lyapunov exponents. In systems whose parameters change adiabatically in time, Ref. [26] provides evidence for such a relation to be appropriate to use. Here we explore the use of such a time-dependent relation for random maps. The characteristic numbers of the snapshot attractors change with time and are found to exhibit large fluctuations. We show that the fluctuations of both the finite time Lyapunov exponents and the information dimension are non-normal. The variance of the former is found to stagnate with increasing ensemble size N, while that of the latter decreases very slowly with N. Furthermore, the Kaplan-Yorke type dimensions evaluated by means of finite time Lyapunov exponents have been found to correlate well with the numerically determined information dimension.

In Sec. II, we review a simple model that exhibits noise-induced chaos. In Sec. III, we show a series of numerically simulated snapshot attractors represented by $N \gg 1$ particles with strong noise. The finite time Lyapunov exponents averaged over ensembles are studied, and the nature of their fluctuations is investigated. Section IV is devoted to the fractal properties of snapshot attractors. Conclusions are presented in

 ©2011 American Physical Society

Sec. V. Details on snapshot chaotic saddles related to snapshot chaotic attractors are relegated to the appendix.

II. MODEL

We consider the noisy version of discrete-time dynamical systems which, in dimensionless form, are written as:

$$\mathbf{x}_{n+1} = \mathbf{f}(\mathbf{x}_n) + \sigma \boldsymbol{\xi}_n, \tag{1}$$

where $\sigma > 0$ represents the noise amplitude and the $\boldsymbol{\xi}$ terms are independent, identically distributed random processes of zero mean and fixed variance. The distribution $P(\boldsymbol{\xi})$ is assumed to be known and to be independent of time so the stochastic process generating the noise is stationary. We shall use a distribution $P(\boldsymbol{\xi})$ that is constant over the finite domain $[-1,1]$. Note that form (1) is somewhat exceptional in the context of snapshot attractors, where noise most typically appears as a modulation of some of the parameters.

To illustrate noise-induced chaos, we consider the invertible map [27]:

$$\begin{aligned} \theta_{n+1} &= \theta_n + 1.32 \sin 2\theta_n - 0.9 \sin 4\theta_n - x_n \sin\theta_n + \sigma \xi_n^{(1)}, \\ x_{n+1} &= -0.9 \cos\theta_n + \sigma \xi_n^{(2)}, \end{aligned} \tag{2}$$

where $\xi_n^{(i)}$ are random variables. Angle θ is taken mod 2π. The deterministic system ($\sigma = 0$) has two coexisting attracting fixed points at $(0,-0.9)$ and $(\pi,0.9)$, respectively. The fixed points are separated by a chaotic saddle whose unstable manifold consists of S-shaped curves, foliations which are approximately orthogonal to those of the basin boundary, as shown in Fig. 1. Noise-induced chaotic attractors obtained at different noise strengths are shown in Fig. 2. At weak noise, the attractor, shown in Fig. 2(a), extends along the fractal unstable manifold of the deterministic chaotic saddle. As the noise strength increases beyond $\sigma_c = 0.02$, the fractal pattern becomes washed out and a fuzzy pattern appears. It has been shown in Refs. [6,7] that noise makes the dynamics space filling on small phase-space scales, less than $\varepsilon_c = 0.018$ for $\sigma = 0.01$. For weak noise, there is always a scaling region, although short, with a slope given by the noise-free fractal dimension of the unstable manifold, which is $D_0 = 1.5$ in this case. When this scaling region disappears, it is no longer possible to identify

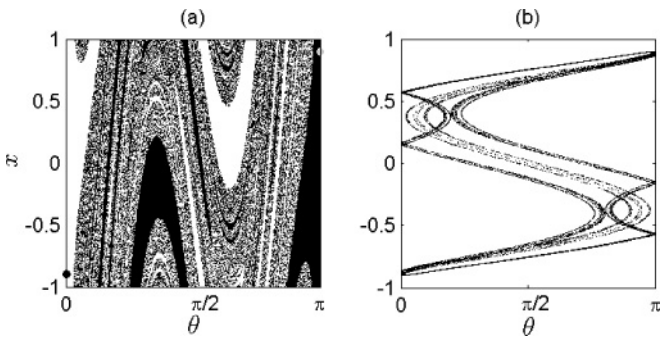

FIG. 1. (a) Two fixed-point attractors and their basins of attraction in the deterministic version ($\sigma = 0$) of map (2) (white/black points are attracted to the large black/blank dot) and (b) the unstable manifold of the chaotic saddle responsible for transient chaos. For plotting, throughout the article, angle θ is taken mod 2π.

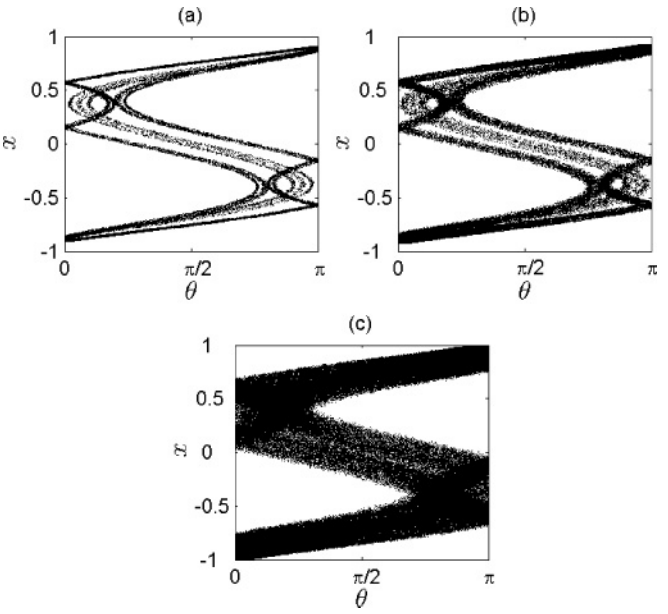

FIG. 2. Noise-induced chaotic attractors in map (2) for various noise strengths: (a) $\sigma = 0.01$, (b) $\sigma = 0.03$, and (c) $\sigma = 0.1$. Single trajectories of lengths (a) about 10^9 (displayed phase-space region partitioned into 1000×1000 boxes, with a maximum of 10 points plotted in each box) and (b) and (c) 10^6 are used to represent the attractors.

the fractality of the noise-induced chaotic attractor. In fact, noise smears out the dynamics into large finite bands of the phase-space. This indicates that noise begins to dominate the dynamics and, when this happens, noise can be considered as strong. Figures 2(b) and 2(c) illustrate such cases. We will consider the latter for our case study. Our aim is to analyze such fuzzy noise-induced chaotic attractors using the concept of snapshot attractors.

III. SNAPSHOT ATTRACTORS

In this section, instead of single long trajectories (as used in Fig. 2) we consider *ensembles* of particles. The random system differs form the deterministic one in that it is not autonomous. If an ensemble is used, the solution for a particular realization of noise can be well represented in the phase-space of the original deterministic system at chosen time instants. Given that the same random perturbation acts on all particles of the ensemble, such a snapshot view of the ensemble is not fuzzy but exhibits fractal patterns [11]. For map (2), Fig. 3 shows a series of subsequent snapshot attractors. The applied noise is strong ($\sigma = 0.1$), the same as in Fig. 2(c). The initial condition for the simulation was an ensemble of $N = 10^5$ randomly scattered particles uniformly distributed in the phase-space region of Fig. 3. After about 20 iterations the particles attain and spread over a phase-space object. The instantaneous form of this object is a snapshot attractor. Each snapshot is a fractal and is similar to the unstable manifold of the chaotic saddle of the deterministic case [Fig. 1(b)]. Here, however, this S-shaped foliation is "randomly" displaced and deformed in time due to the strong noise.

In general, the form of the natural distribution of snapshot attractors also depends on the time instant. In case of the

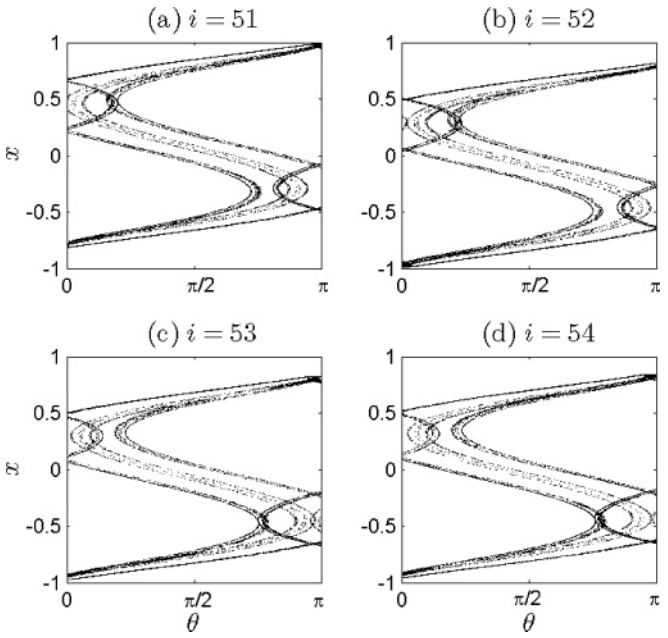

FIG. 3. A series of subsequent snapshot attractors for strong noise ($\sigma = 0.1$), corresponding to Fig. 2(c). In the respective panels the snapshots were taken at the indicated iteration numbers i. An ensemble of $N = 10^5$ trajectories were used with randomly assigned initial conditions in the phase-space domain: $\theta \in [0,\pi]$, $x \in [-1,1]$.

considered map, however, one feature of this natural measure is invariant: high peaks near the attracting fixed points of the deterministic system. This is highlighted in Fig. 4. The stable fixed points and their neighborhood become part of the snapshot attractor; from here the particles occasionally visit the regions where the chaotic saddle used to be, but soon after they return. The dynamics is thus strongly intermittent. The distribution, nevertheless, does have a fractal nature all over the support.

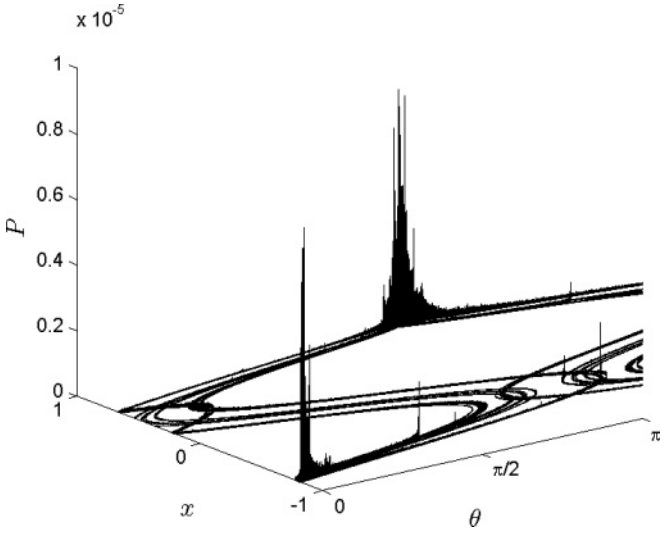

FIG. 4. Typical natural (normalized) distribution P over a snapshot attractor. The applied noise is strong ($\sigma = 0.1$). The present resolution was achieved by using a number of $N = 10^6$ points and a number of 5000 bins in both directions.

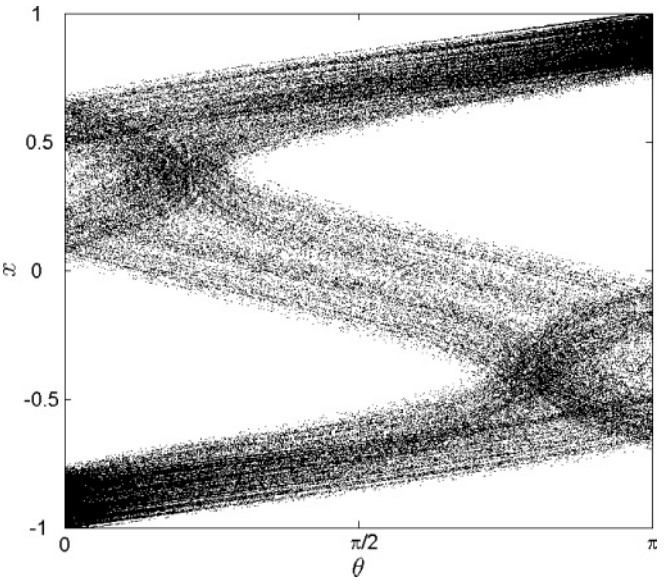

FIG. 5. A series of 100 subsequent snapshot attractors plotted in one diagram. The series starts from iteration number $i = 50$, and the noise is strong ($\sigma = 0.1$). Every snapshot is constituted by 10^4 points; thus the collective plot consists of 10^6 points. The pattern is practically identical to that of Fig. 2(c).

If snapshot attractors are overlayed in one diagram, the pattern that appears is similar to the noise-induced chaotic attractor obtained from a single very long trajectory of the random map (2). Such a collective plot of $M = 100$ subsequent snapshots can be seen in Fig. 5. Indeed, this is practically the same as Fig. 2(c): the fractality is completely destroyed, the points being area filling. To realize a similar density with 10^6 points in the two figures, every snapshot attractor is constituted by $N = 10^4$ points. It is noted that the resulting picture is qualitatively the same when overlaying 10 times more, that is, $M = 1000$ snapshots (with $N = 10^3$ points all), or when taking only every 50th snapshot attractors, that is, taking $i = 50m + 1$, $m = 1,2,\ldots,M$, $M = 100$ (with $N = 10^4$ points all).

The coincidence of Figs. 2(c) and 5 is easy to interpret in the latter case. The overlay contains the union of N trajectories of total length $50M + 1$. For large M, every individual trajectory is very long and provides a faithful representation of the noisy system's attractor. Due to ergodicity, the union of N such trajectories only repeats the pattern, and therefore we expect for $M \gg 1$ the overlaid pattern to coincide with the noise-induced chaotic attractor. Our numerical finding illustrates that $M = 100$ is already a sufficiently large number for this purpose.

The natural distribution of the noise-induced chaotic attractor, represented by a single long trajectory, is displayed in Fig. 6. In view of the argument above, it is expected to be obtained as the superposition of several snapshot natural distributions, like the one in Fig. 4. All these observations prove that the snapshot attractors can be considered to be the fractal building blocks of fuzzy noise-induced chaotic attractors.

To reveal the time-dependent character of the snapshot attractors, next we turn our attention to the dynamical

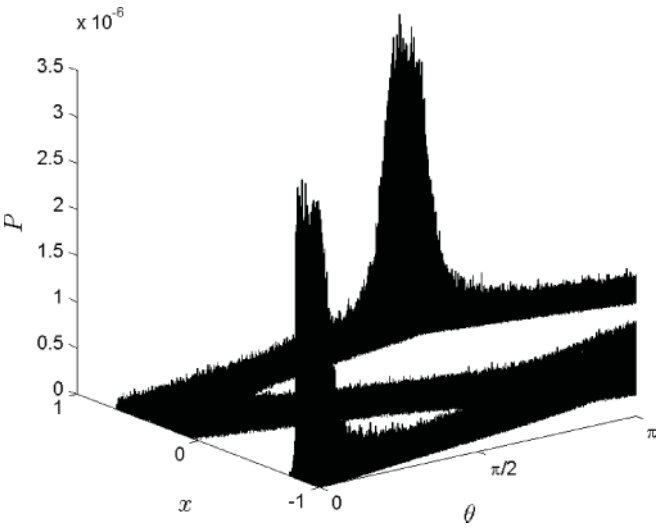

FIG. 6. The natural (normalized) distribution P of the fuzzy noise-induced chaotic attractor of Fig. 2(c). The present resolution was achieved by using a number of $N = 10^6$ points and a number of 1000 bins in both directions.

instability on the attractor, which is characterized by the local or finite time Lyapunov exponents (FTLE) [28]. The largest FTLE was numerically approximated by following the major axis of the error ellipsoid as it grows for each trajectory. If the growth factor [29] of this axis in the jth step is denoted by y_j, then the largest FTLE [$\lambda^{(n)}$] at time i is calculated as:

$$\lambda^{(n)} = \frac{1}{n}\sum_{j=i}^{i+n} \ln y_j; \tag{3}$$

that is, the finite time mean of growth over n steps, where the superscript (n) indicates the length of time over which the Lyapunov exponent is evaluated. The y_j's are determined from the Jacobian matrix of map (2). In two-dimensional maps the determinant of the Jacobian matrix, $J^{(n)}$, of the n-fold-iterated map can be used to exactly relate the smaller negative FTLE $\lambda'^{(n)}$ to the larger one via the relation [30,31]:

$$\lambda^{(n)} + \lambda'^{(n)} = \frac{1}{n}\ln[J^{(n)}] = \frac{1}{n}\sum_{j=i}^{i+n} \ln(J_j). \tag{4}$$

Here J_j denotes the Jacobian in the jth step: $J_j = J(\mathbf{x}_j)$, where J is the Jacobian determinant of map (2) evaluated at $\mathbf{x}_j = (\theta_j, x_j)$.

We evaluated FTLE's, $\lambda^{(n)}$ and $\lambda'^{(n)}$, for various n's. In Fig. 7, FTLE's, averaged over ensembles that represent the attractor, for $n = 20$ and $n = 100$ are displayed as functions of time. [Note that Eqs. (3) and (4) are formulated for single trajectories, but all other occurrences of $\lambda^{(n)}$ and $\lambda'^{(n)}$ shall denote ensemble averages throughout the article.] Results are presented for two ensemble sizes: $N_1 = 10^5$ and $N_2 = 10^6$. Corresponding pairs of time series overlap in the diagrams, hence they are undistinguishable. The following conditions were imposed to this and all simulations discussed in this article: the same noise realization is retained and different random initial ensembles are used, representing a uniform distribution over the phase-space domain: $\theta \in [0,\pi]$, $x \in [-1,1]$.

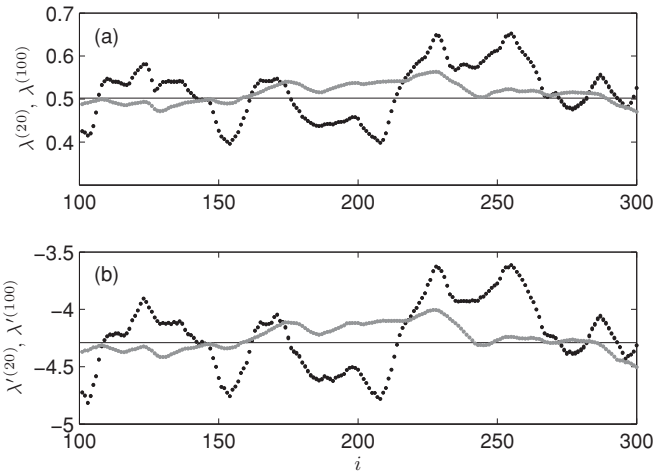

FIG. 7. Time dependence of the FTLE's, (a) $\lambda^{(n)}$ and (b) $\lambda'^{(n)}$, with $n = 20$ (black) and $n = 100$ (gray). Time series obtained using $N_1 = 10^5$ and $N_2 = 10^6$ overlap in the diagrams. The same noise realization was used for all time series, and it is retained throughout the article. Horizontal lines represent the long-time-averaged Lyapunov exponents: $\bar{\lambda} = 0.502$ and $\bar{\lambda}' = -4.29$.

The respective time series of the positive [Fig. 7(a)] and negative average FTLE's [Fig. 7(b)] take similar shapes; although the fluctuations of the $\lambda^{(n)}$'s are smaller than those of the $\lambda'^{(n)}$'s. Also, fluctuations decrease with increasing n.[1]

As a result of assessing the effect of increasing ensemble size it is observed that (i) the shapes of the time series of $\lambda^{(n)}$ and $\lambda'^{(n)}$ are practically preserved and (ii) the magnitude of fluctuation hardly changes. In particular, for the FTLE's the fluctuation appears to stagnate with increasing N (see Table I and related discussions). These results are surprising because in the deterministic case the variance of the FTLE's decrease markedly with increasing ensemble size N.

Points (i) and (ii) are indicators of non-normal fluctuations. For normal fluctuations the following law should apply [32]:

$$\frac{\sigma_1^2}{\sigma_2^2} = \frac{N_2}{N_1}. \tag{5}$$

Here, indices refer to two arbitrarily chosen particle numbers N_1 and N_2; and the σ's are the standard deviation of the distribution under consideration. Law (5) holds more accurately when larger and more distinct N's are chosen.

The temporal averages of the FTLE's are found to stabilize at a value of $\bar{\lambda} = 0.502$ and $\bar{\lambda}' = -4.29$ after about 10^6 iterations. To obtain these figures five different long trajectories were used, and (3) was evaluated with $i = 0$, $n = 10^6$. The long time needed is presumably due to the strongly intermittent dynamics.

Statistics for time series longer than those displayed in Fig. 7 are presented in Table I. The FTLE's are measured for 1000 iterations, which, as a long time series, is broken down into five blocks of 200 iterations each (b1,. . .,b5, where b1

[1]Results for $\lambda'^{(20)}$ obtained by means of the Gram-Schmidt orthogonalization technique (not shown) are in good agreement with that of Fig. 7.

TABLE I. Statistics for the temporal means of $\bar{\lambda}^{(20)}$, $\bar{\lambda}^{(100)}$. Figures in the columns labeled b1,. . .,b5 correspond with subsequent trajectory sections of over 200 iterations. The figures are given up to four digits for the purpose of comparison. By increasing $N_1 = 10^5$ to $N_2 = 10^6$, the corresponding figures of standard deviation [$\sigma_{\bar{\lambda}^{(n)}}$ and $\sigma_{\bar{\lambda}'^{(n)}}$], blockwise and overall, are found to match very closely.

N	b1	b2	b3	b4	b5	Overall
			$\bar{\lambda}^{(20)}$			
10^5	0.5180	0.4838	0.5151	0.5360	0.4996	0.5105
10^6	0.5181	0.4841	0.5150	0.5355	0.4999	0.5105
			$\sigma_{\bar{\lambda}^{(20)}}$			
10^5	0.0634	0.0989	0.0778	0.0757	0.0712	0.0801
10^6	0.0631	0.0990	0.0778	0.0763	0.0720	0.0803
			$\bar{\lambda}^{(100)}$			
10^5	0.5142	0.4776	0.5233	0.5329	0.4831	0.5062
10^6	0.5137	0.4777	0.5233	0.5328	0.4833	0.5062
			$\sigma_{\bar{\lambda}^{(100)}}$			
10^5	0.0223	0.0202	0.0222	0.0206	0.0367	0.0334
10^6	0.0224	0.0203	0.0221	0.0204	0.0364	0.0332

corresponds to Fig. 7). This facilitates a means to provide a statistics of the mean and standard deviation (s.d.) of the blockwise averages. The blockwise and overall comparison of both the mean and s.d. values for the considered characteristic numbers reveals that the increasing ensemble size makes a difference only in roughly the fourth digit after the decimal point. However, when figures are considered across the blocks, we see fluctuations and give conservative estimates such as, $\bar{\lambda}^{(20)} = 0.51 \pm 0.02$, $\bar{\lambda}^{(100)} = 0.51 \pm 0.02$, and, in a similar way, based on data not shown, $\bar{\lambda}'^{(20)} = -4.3 \pm 0.15$, $\bar{\lambda}'^{(100)} = -4.3 \pm 0.15$. These temporal averages over time intervals of length 200 are found to be quite close to the long-time averages, $\bar{\lambda}^{(20)} = 0.505 \pm 0.001$, $\bar{\lambda}^{(100)} = 0.502 \pm 0.001$, $\bar{\lambda}'^{(20)} = -4.285 \pm 0.005$, $\bar{\lambda}'^{(100)} = -4.293 \pm 0.005$, which are estimated on the basis of a few simulations iterating a single initial value over 10^6 steps and using different realizations of noise. It is noted that the very good blockwise agreement is due to the identical condition imposed as highlighted above, namely retaining the same noise realization. This way the major contributor to the fluctuation across the blocks is due to the different noise realization.

For a reference, we carried out control simulations with the random baker map studied as *Case I* in Ref. [11]. Statements (i) and (ii) above are found to apply also in this case, indicating that these features are typical of any random map. An explanation is the following. Snapshot attractors are constructed from an ensemble of trajectories, and ensemble averages can be evaluated over them. However, temporal averages cannot be defined on any individual snapshot. Hence, ergodicity in terms of the equivalence of ensemble and temporal averages is not meaningful. Temporal averages, nevertheless, can be defined over long times, i.e., over the noise-induced chaotic attractor. The ensemble average of any quantity taken over finite-time noise realizations might thus be time dependent and might differ from the overall temporal average. By considering the union of all possible noise realizations, however, ergodicity is recovered and holds for the noise-induced chaotic attractor. In other words, ergodicity in terms of a unique stationary distribution implies in the nonrandom case that finite-time ensemble averages rapidly converge to the long-time average and that their temporal fluctuations are vanishing with increasing ensemble size. Such an implication does not apply in the random case when finite sequences of noise realization are investigated.

IV. FRACTAL PROPERTIES

The Lyapunov dimension D_L of deterministic chaotic attractors can be expressed via the Kaplan-Yorke formula [30]:

$$D_L = 1 + \frac{\bar{\lambda}}{|\bar{\lambda}'|}, \tag{6}$$

where $\bar{\lambda}$ and $\bar{\lambda}'$ are the positive and negative time-averaged Lyapunov exponents on the attractor. For typical snapshot attractors the same expression has been proven [11,25] to hold, where $\bar{\lambda}$ and $\bar{\lambda}'$ are the positive and negative time-averaged Lyapunov exponents on the noisy chaotic attractor. With the average Lyapunov exponents determined numerically in the noisy system, the Lyapunov dimension (6) yields as $D_L = 1.117$ for our snapshot attractors at strong noise ($\sigma = 0.1$). The dimension of the noise-induced chaotic attractor at weak noise, however, is provided by another expression [6,7]. The relation and the crossover between these expressions is discussed in the appendix.

Next, we introduce—in a similar way as in Ref. [26]—"finite-time" Lyapunov dimensions:

$$D_L^{(n)} = 1 + \frac{\lambda^{(n)}}{|\lambda'^{(n)}|}, \tag{7}$$

based on the FTLE's $\lambda^{(n)}$ and $\lambda'^{(n)}$. We evaluated such dimensions and compared them with a direct calculation of the information dimension D_1. Note that the $n \to \infty$ limit of $D_L^{(n)}$ is expected to coincide with D_L (which tendency is also supported by data provided in the caption of Fig. 11).

In Fig. 8 the time dependencies of $D_L^{(20)}$ and $D_L^{(100)}$ are shown. Ensemble sizes $N_1 = 10^6$ and $N_2 = 10^7$ are used, and corresponding pairs of time series are again undistinguishable, and properties (i) and (ii) hold.

Figure 9 exhibits the time series of the information dimension D_1 calculated according to the standard definition [30] after every iteration of a snapshot attractor, with the use of $N_1 = 10^6$ and $N_2 = 10^7$ particles. The root-mean-square error (rmse) of the fitting of the scaling line (not shown) is found

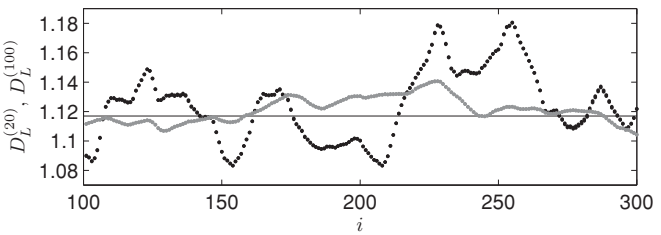

FIG. 8. Time series of the finite time Lyapunov dimensions $D_L^{(20)}$ (black) and $D_L^{(100)}$ (gray). Time series obtained using $N_1 = 10^6$ and $N_2 = 10^7$ overlap in the diagrams. A horizontal line indicates the long-time average $D_L = 1.117$.

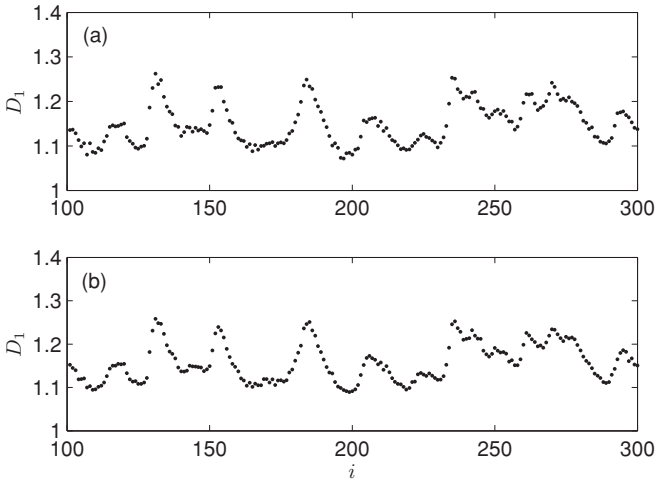

FIG. 9. Time series of the information dimension D_1 (calculated directly) using a number of (a) $N_1 = 10^6$ and (b) $N_2 = 10^7$ particles for the ensemble. The scaling lines were fitted on the longest possible range with acceptable rmse figures (<0.04 most typically) of widths about (a) 90 and (b) 160.

to be most typically less than 0.04. Properties (i) and (ii) hold also for the time series of D_1.

Statistics for longer time series than those displayed in Fig. 9 are presented in Table II for the same noise realization as in Table I, but here particle numbers $N_1 = 10^6$ and $N_2 = 10^7$ are considered. Based on the provided data of temporal fluctuations a conservative estimate of $\bar{D}_1$ is given such as $\bar{D}_1 = 1.16 \pm 0.02$. A further source of inaccuracy is due to the fitting of the scaling line, which yields an additional error of ± 0.04, i.e., $\bar{D}_1 = 1.16 \pm 0.06$. To maintain the same conditions in this case, nevertheless, we also used the same range of fitting in cases of both $N_1 = 10^6$ and $N_2 = 10^7$, with which, blockwise and overall, practically no difference between the s.d. values is found, similarly to the case of the Lyapunov exponents (cf. Table I). Concerning the s.d. values obtained with the extended range provided by the increase of the particle number N, a weak decrease of σ_{D_1} can be observed.

It is worth recalling an observation of Namenson *et al.* [14] according to which the fluctuations of the information dimension in random maps has a variance $\sigma_{D_1} \sim [\ln(1/\epsilon_*)]^{-1/2}$, where ϵ_* represents the smallest box size reasonable to use in a box counting algorithm. It is easy to convert this size to the number of particles in the ensemble. Let N_0 denote the average number of particles needed to have a reasonable statistics in each box, say $N_0 = 100$. Since the number $N(\epsilon)$ of boxes needed to cover the snapshot attractor is $N(\epsilon) = H\epsilon^{-D_0}$, where D_0 is the fractal dimension and H the Hausdorff measure, ϵ_* follows from the constraint $N_0 H {\epsilon_*}^{-D_0} = N$. Thus, $\ln \epsilon_* \sim \ln(N/HN_0)$, and for large N we have

$$\frac{\sigma^2_{D_1,1}}{\sigma^2_{D_1,2}} \approx \frac{\ln N_2}{\ln N_1}. \tag{8}$$

This represents a particular form of non-normal fluctuations and implies an extremely slow convergence to zero. Our data for the information dimension calculations appear to be consistent with this law.

We thus conclude that neither the Lyapunov dimensions $D_L^{(n)}$ expressed by means of finite time Lyapunov exponents (Table I) nor the direct computation of the information dimension (Table II) exhibit normal fluctuations. In addition, there is a small but measurable difference, on the order of a few percentage points, between the traditional Lyapunov dimension D_L (6) and $\bar{D}_1$. We attribute this to the strongly intermittent, nonhyperbolic dynamics on the snapshot attractors or to the unavoidable finite number N of particles representing the ensemble. By including a conservative estimate of the errors, however, an agreement between D_L and $\bar{D}_1$ cannot be excluded.

An interesting relation can be discovered when cross correlations are calculated between the time series of D_1 and $D_L^{(n)}$. In Fig. 10(a) we find that they are correlated as indicated

TABLE II. Statistics for the temporal means of $\bar{D}_1$, in a similar way as with Table I. For $N_2 = 10^7$ two sets of figures are displayed; the upper one corresponds to a range of fitting used in the case of $N_1 = 10^6$ and the lower one was obtained by using the possible longest range of fitting.

N	b1	b2	b3	b4	b5	Overall
			$\bar{D}_1$			
10^6	1.15	1.13	1.15	1.16	1.15	1.15
10^7	1.16	1.15	1.16	1.17	1.16	1.16
10^7	1.16	1.14	1.16	1.17	1.16	1.16
			σ_{D_1}			
10^6	0.046	0.066	0.053	0.051	0.047	0.054
10^7	0.046	0.066	0.054	0.051	0.047	0.054
10^7	0.044	0.062	0.051	0.049	0.044	0.051

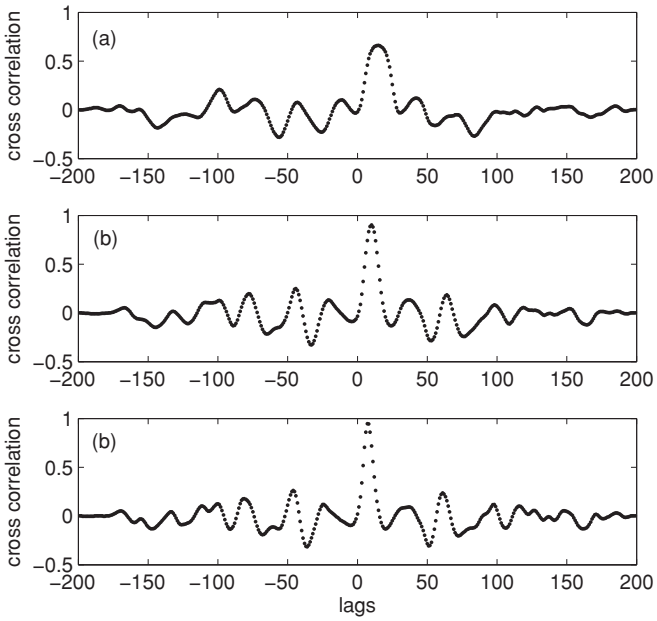

FIG. 10. Cross correlations of the information dimension D_1 with the Lyapunov dimension $D_L^{(n)}$ for (a) $n = 20$, (b) $n = 10$, and (c) $n = 5$. The time series were scaled by the standard deviation before taking their normalized cross correlation so a perfect match would lead to 1 at the maximum.

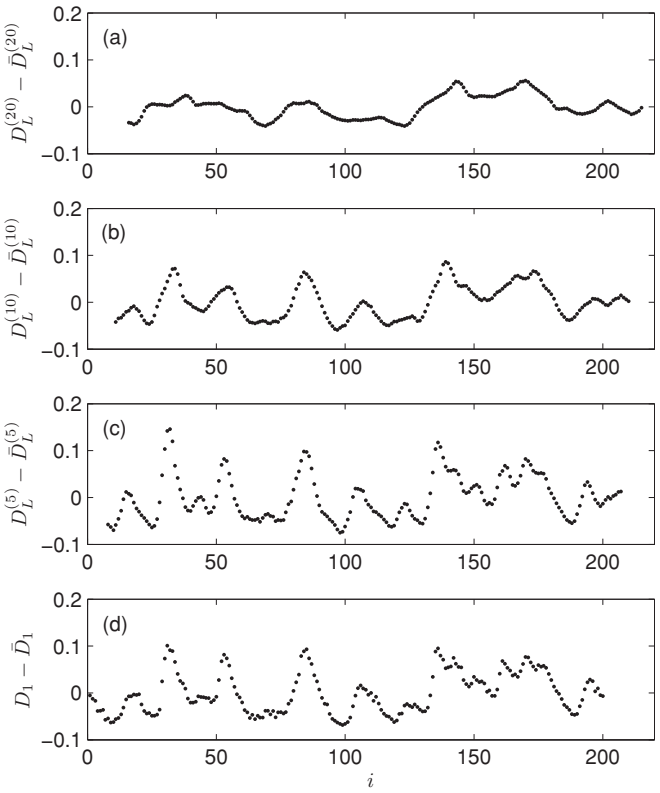

FIG. 11. Time series of the Lyapunov dimension $D_L^{(n)}$ for (a) $n = 20$, (b) $n = 10$, and (c) $n = 5$. The time series of a direct calculation of the information dimension D_1 [taken from Fig. 9(b)], with which the cross correlations were constructed for Fig. 10, is included in the bottom for reference. The upper three sequences are shifted in the positive direction along the abscissa by $\Delta i = 15, 9, 7$, for $n = 20$, 10, and 5, respectively, where Δi's are the locations of the peaks in Fig. 10. This way corresponding peaks of the sequences align. The mean values subtracted before taking the cross correlation are $\bar{D}_L^{(20)} = 1.1242$, $\bar{D}_L^{(10)} = 1.1265$, $\bar{D}_L^{(5)} = 1.1288$, and $\bar{D}_1 = 1.16$.

by a peak. For decreasing n [Figs. 10(b) and 10(c)], the cross correlation is stronger and stronger. This effect is displayed in Fig. 11 in terms of the time series themselves. Note that before taking the cross correlation the mean of each sequence was subtracted, which differs in each case. Note also that for greater n's the sequence tends to be smoother and the fluctuation is smaller, which is consistent with taking averages over longer times.

The observed correlation confirms that a time-dependent version of the Kaplan-Yorke relation (7) has a specific meaning for finite ensemble size N: $D_L^{(n)}$ for some small value of n provides a good approximation of the numerically determined D_1. This strong correlation is remarkable, considering that the algorithms by which they are obtained are entirely unrelated. A detailed analysis shows that the cross correlation is maximal at $n^* = 6$ ($n^* = 4$ for the random baker map). This might be interpreted such that, with the ensembles used, the last n^* iterations dominate in determining the information dimension of a snapshot attractor. The value of n^* is thus expected to be a (slowly varying) function of N.

Next, we consider the fractal dimension D_0. Qualitative properties of the time series obtained for D_0 (not shown)

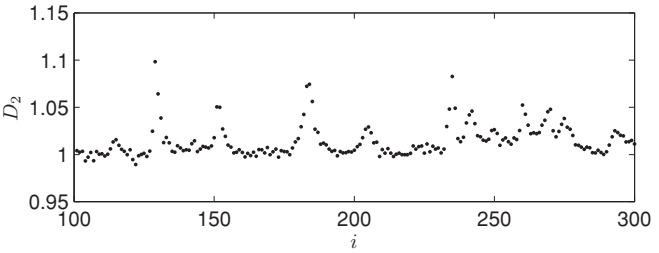

FIG. 12. A time series of the correlation dimension D_2 calculated directly. The rmse of fitting the scaling line is most typically smaller than 0.02. For the ensemble a number of $N = 10^4$ particles were used.

are similar to those of D_1. The rmse values of fitting are typically somewhat smaller than those for D_1. These suggest that properties (i) and (ii) do apply, but the s.d. values (not shown) are much smaller. As a conservative estimate, including fluctuations of the mean due to different noise realizations as well as inaccuracies due to fitting the scaling line, we give here as $\bar{D}_0 = 1.53 \pm 0.04$, in which error the latter contribution dominates.

We also investigated the correlation dimension D_2 of the snapshot attractors. The time series of D_2 with $N = 10^4$ is displayed in Fig. 12. The typical value is about 1, and the rmse of fitting is most typically smaller than 0.02; that is, the scaling line of the correlation integral is a very straight line, even if using as few particles as $N = 10^4$. As a conservative estimate, we find $\bar{D}_2 = 1.02 \pm 0.02$.

The explanation for the rather distinct value of D_2 from that of D_1 and D_0 is that the correlation dimension can be seen as a biased fractal dimension giving a larger weight to more densely populated regions of the fractal. As shown by Fig. 4 such pronounced parts of the snapshot attractors are around the fixed points. Since the support here is more a simple line than a fractal, the local dimension is close to 1 and dominates D_2. Because these peaks of the natural distribution are very robust, the rmse can stay small. The presence of these peaks also explains our finding (not shown) that the standard deviation of D_1 due to different noise realizations is about one order of magnitude larger than that of the fractal dimension D_0 since the latter is not sensitive to the irregularities of the natural distribution.

V. CONCLUSIONS

We have pointed out that a fuzzy noise-induced chaotic attractor at strong noise can be decomposed into an infinite set of fractal snapshot attractors. The snapshot attractors arise from ensembles of particles subject to the same noise realization and produce clear fractal patterns after relatively short random sequences. We have found that the overlay of about 100 different snapshot attractors produces in practice a rather good approximant to the noise-induced chaotic attractor.

The investigation of time series of ensemble averages of physical quantities revealed that (i) for a given realization of noise the time series of the averages are largely independent of the size and realizations of the ensemble of initial conditions. Furthermore, (ii) the variance of finite time quantities, like, e.g., the Jacobian determinant

or the finite time Lyapunov exponents, is found to remain finite, while those of the dimensions decrease slowly when increasing the size of the ensembles. These findings lead to the conclusion that these characteristic numbers exhibit non-normal fluctuations.

One often reads in the literature on snapshot attractors that—although they change their shape in time—they possess a time-independent information dimension given by the Kaplan-Yorke formula [30]. Our experience shows that the average Lyapunov exponents and the Kaplan-Yorke formula can be obtained from very long temporal sequences only. The information dimension of the snapshot attractors determined directly show considerable fluctuations, and even its temporal average over finite time intervals might deviate (a few percentage points) from the Kaplan-Yorke results. We evaluated the Kaplan-Yorke dimension based on finite time Lyapunov exponents of length n as well. Such a Kaplan-Yorke dimension happens to exhibit the most similar fluctuations to that of the directly evaluated information dimension when n is as low as about 6. This finding confirms that with any accessible ensemble size, fluctuations of the information dimension are non-normal and that the last few iterations appear to influence the information dimension of a snapshot attractor the most.

Note added in proof. We thank A. Endler for calling our attention to a paper [34] and a response to it by [35], which describe non-normal fluctuations of ensembles in a different context.

ACKNOWLEDGMENTS

This work was supported by the Hungarian Science Foundation under Grant No. OTKA NK72037. The project is also supported by the European Union and is cofinanced by the European Social Fund (Grant No. TAMOP 4.2.1./B-09/KMR-2010-0003). Useful discussions with E. G. Altmann are acknowledged.

APPENDIX: SNAPSHOT CHAOTIC SADDLES AS BUILDING BLOCKS OF SNAPSHOT ATTRACTORS

In the weak-noise limit, the information dimension of the noise-induced attractor in two-dimensional maps can be approximated by the information dimension of the unstable manifold of the saddle of the deterministic case [6,7] such that

$$D_L = 1 + \frac{\bar{\lambda} - \kappa}{|\bar{\lambda}'|}, \tag{A1}$$

where κ is the escape rate of the deterministic chaotic saddle. Note that this dimension is independent of the noise strength σ in the weak-noise limit.

Equation (A1) does not apply to noise-induced attractors at strong noise ($\sigma > \sigma_c$). In that case there is no deterministic chaotic saddle whose unstable manifold would form a basic element of the noise-induced or of the snapshot attractors. If, however, the dynamics is leaked [33] by defining holes of radius δ around the fixed points, and a given realization of the noise is applied to an ensemble of particles, a snapshot chaotic saddle arises.

Figure 13 shows a series of a few such snapshots for strong noise ($\sigma = 0.1$), constructed as follows. In a box that contains

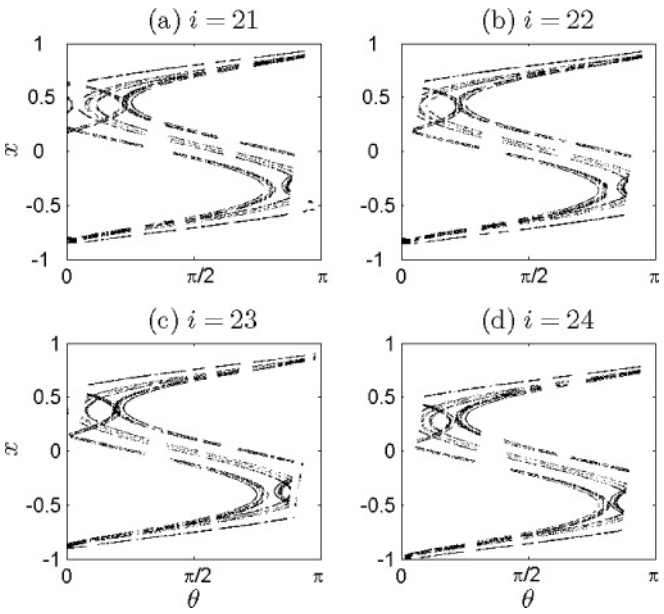

FIG. 13. A series of subsequent snapshots of chaotic saddles for strong noise ($\sigma = 0.1$). The applied leak size is $\delta = 0.01$.

the snapshot attractor an ensemble of randomly distributed particles is taken at zero time. Then the map system (2) is applied over 40 iterations. After each iteration a particle escapes if it enters any of the leaks of size δ around the fixed points. The fixed point is located numerically by searching for the (local) maximum of the probability distribution. Those particles which have not entered the leaks after 40 iterations represent the unstable manifold of the snapshot chaotic saddle. The same particles on the initial configuration represent the stable manifold. These same particles approach closely the snapshot saddle at some point in the meantime (we created snapshots halfway: at iteration 20), and they are therefore taken to represent the saddle [31]. For subsequent snapshots the procedure was shifted along the predefined random sequence of noise. It can be seen in Fig. 13 that the geometry changes slightly over the iterations, similarly as in Fig. 3, but the double fractal structure typical of chaotic saddles is persistent.

For such a random chaotic saddle a mean value of the dynamical measures such as the escape rate and the Lyapunov exponents can be taken, and they are linked by a formally identical relation with (A1).

As the escape of the majority of particles happens over some tens of iterations, and because the fluctuations are characterized on comparable time scales, the escape rate could be difficult to estimate.[2] This difficulty can be overcome by averaging the number $N(i)$ of nonescaped particles versus the iteration number i for a number of independent simulations using different realizations of noise. This way we estimated the mean escape rate (κ) for various values of the leak size (δ) and obtained a *monotonous relation*. That is, there is no uniquely defined random chaotic saddle for strong noise whose characteristic numbers are to be substituted into Eq. (A1); for differ-

[2]This also means that a time-dependent version of relation (A1) is difficult to support numerically.

ent δ's different subsets of the snapshot attractor act as snapshot saddles. In the weak noise limit ($\sigma < \sigma_c = 0.02$ in our case) κ does not depend on small values of δ, which indicates the existence of a unique set of snapshot chaotic saddles, whose mean escape rate is approximately the same as the escape rate in the deterministic case. Therefore, while in the weak noise limit Eq. (A1) applies because there is a unique random chaotic saddle, it does not apply in the case of strong noise because random chaotic saddles can be defined only via an artificial leaking of the dynamics. Instead, the $\delta \to 0$, $\kappa \to 0$ limit should be considered (that is, the case of snapshot attractors) with which Eq. (A1) transforms into the Kaplan-Yorke relation (6).

[1] M. Iansiti, Q. Hu, R. M. Westervelt, and M. Tinkham, Phys. Rev. Lett. **55**, 746 (1985).

[2] H. Herzel, W. Ebeling, and T. Schulmeister, Z. Naturforsch. A **42**, 136 (1987).

[3] A. R. Bulsara, W. C. Schieve, and E. W. Jacobs, Phys. Rev. A **41**, 668 (1990).

[4] T. W. Carr, L. Billings, I. B. Schwartz, and I. Triandaf, Physica D **147**, 59 (2000); L. Billings and I. B. Schwartz, J. Math. Biol. **44**, 33 (2002); L. Billings, E. M. Bollt, and I. B. Schwartz, Phys. Rev. Lett. **88**, 234101 (2002); E. Bollt, L. Billings, and I. Schwartz, Physica D **173**, 153 (2002); E. Forgoston, L. Billings, and I. B. Schwartz, Chaos **19**, 043110 (2009).

[5] Y.-C. Lai, Z. Liu, L. Billings, and I. B. Schwartz, Phys. Rev. E **67**, 026210 (2003); B. Xu, Y.-C. Lai, L. Zhu, and Y. Do, Phys. Rev. Lett. **90**, 164101 (2003).

[6] T. Tél, Y.-C. Lai, and M. Gruiz, Int. J. Chaos Bif. **18**, 509 (2008).

[7] T. Tél, and Y.-C. Lai, Phys. Rev. E **81**, 056208 (2010).

[8] B. Xu, Y.-C. Lai, L. Zhu, and Y. Do, Phys. Rev. Lett. **90**, 164101 (2003).

[9] D. A. Rand and H. B. Wilson, Proc. R. Soc. London Ser. B **246**, 179 (1991).

[10] S. P. Ellner and P. Turchin, Oikos **111**, 620 (2005).

[11] F. J. Romeiras, C. Grebogi, and E. Ott, Phys. Rev. A **41**, 784 (1990).

[12] L. Yu, E. Ott, and Q. Chen, Phys. Rev. Lett. **65**, 2935 (1990); Physica D **53**, 102 (1991).

[13] J. C. Sommerer and E. Ott, Science **259**, 335 (1993).

[14] A. Namenson, E. Ott, and T. M. Antonsen, Phys. Rev. E **53**, 2287 (1996).

[15] J. Jacobs, E. Ott, T. Antonsen, and J. Yorke, Physica D **110**, 1 (1997).

[16] Z. Neufeld and T. Tél, Phys. Rev. E **57**, 2832 (1998).

[17] G. Károlyi, T. Tél, A. P. S. de Moura, and C. Grebogi, Phys. Rev. Lett. **92**, 174101 (2004).

[18] Y.-C. Lai, U. Feudel, and C. Grebogi, Phys. Rev. E **54**, 6070 (1996).

[19] Y.-C. Lai, Phys. Rev. E **60**, 1558 (1999).

[20] E. G. Altmann and A. Endler, Phys. Rev. Lett. **105**, 244102 (2010).

[21] C. S. Rodrigues, C. Grebogi, and A. P. S. de Moura, Phys. Rev. E **82**, 046217 (2010).

[22] L. Arnold, *Random Dynamical Systems* (Springer-Verlag, Berlin, 1998).

[23] M. Ghil, M. D. Chekroun, and E. Simonnet, Physica D **327**, 2111 (2008).

[24] M. D. Chekroun, E. Simonnet, and M. Ghil, Stochastic climate dynamics: Random attractors and time-dependent invariant measures, preprint, 2010.

[25] F. Ledrappier and L.-S. Young, Commun. Math. Phys. **17**, 529 (1988).

[26] R. Serquina, Y.-C. Lai, and Q. Chen, Phys. Rev. E **77**, 026208 (2008).

[27] S. W. McDonald, C. Grebogi, E. Ott, and J. Yorke, Physica D **17**, 125 (1985).

[28] G. Boffetta, M. Cencini, M. Falcioni, and A. Vulpiani, Phys. Rep. **356**, 367 (2002).

[29] K. T. Alligood, T. D. Sauer, and J. A. Yorke, *Chaos* (Springer, New York, 2005).

[30] E. Ott, *Chaos in Dynamical Systems* (Cambridge University Press, Cambridge, 1991).

[31] T. Tél and M. Gruiz, *Chaotic Dynamics* (Cambridge University Press, Cambridge, 2006).

[32] L. E. Reichl, *A Modern Course in Statistical Physics* (John Wiley & Sons, New York, 1998).

[33] J. Schneider, T. Tél, and Z. Neufeld, Phys Rev. E **66**, 066218 (2002).

[34] Sinha, Phys. Rev. Lett. **69**, 3306 (1992).

[35] Pikovsky, Phys. Rev. Lett. **71**, 653 (1993).